

## WALL $y^+$ APPROACH FOR DEALING WITH TURBULENT FLOW OVER A SURFACE MOUNTED CUBE: PART 2 – HIGH REYNOLDS NUMBER

Mohd ARIFF, Salim M. SALIM\* and Siew Cheong CHEAH

Department of Mechanical, Materials and Manufacturing Engineering,  
University of Nottingham (Malaysia Campus), Semenyih, 43500, Selangor, MALAYSIA

\*Corresponding Author, Email address: keyx8sms@nottingham.edu.my

### ABSTRACT

An approach for dealing with turbulent flows over a surface-mounted cube using the wall  $y^+$  as guidance in selecting the appropriate grid configuration and corresponding turbulence models are investigated using Fluent. The study is divided into two parts- Part I and Part II, dealing with low and high Reynolds number, respectively. Part I dealt with a low Reynolds number of 1,870. In Part II presented here, a Reynolds number of 40,000 based on cube height and bulk velocity is investigated and the computational results are compared with experimental data from Martinuzzi et al. (1993) on 'the flow around surface-mounted, prismatic obstacles placed in a fully developed channel flow'. The standard  $k-\varepsilon$ , standard  $k-\omega$ , Reynolds Stress Model (RSM), Spalart-Allmaras (SA) and renormalization group (RNG)  $k-\varepsilon$  models are used to solve the closure problem. Their behaviour together with the accompanying near-wall treatments is investigated for wall  $y^+ \approx 5$  covering the viscous sublayer,  $y^+ \approx 22$  the buffer region and  $y^+ \approx 33$  resolving the log-law region, unlike the previous study (Part I – Ariff et al., 2009) which could only resolve the viscous sublayer and buffer region due to the comparatively lower Reynolds number. It is concluded that the mesh resolving the log-law region is sufficiently accurate without incurring additional computational cost. RSM turbulence model best predicts the flow separation region above the cube whereas the standard  $k-\varepsilon$  performs better in the flow reattachment and recovery regions.

### NOMENCLATURE

D	Domain Depth (m)
H	Height of Obstacle (m)
L	Length of the channel (m)
u	Instantaneous Velocity ( $\text{ms}^{-1}$ )
$u_B$	Bulk Velocity ( $\text{ms}^{-1}$ )
$u_\tau$	Friction Velocity ( $\text{ms}^{-1}$ )
x	Horizontal Distance along Streamwise direction (m)
$X_F$	Frontal Separation length (H)
$X_R$	Reattachment Length (H)
y	Vertical Distance normal to wall direction (m)
z	Distance parallel to the spanwise direction (m)
$Re_H$	Reynolds Number (= $Hu_B/\nu_{air}$ )
$y^+$	Dimensionless distance to the wall
k	Turbulent kinetic energy ( $\text{m}^2 \text{s}^{-2}$ )
$\nu_{air}$	Kinematic viscosity of air ( $\text{m}^2 \text{s}^{-1}$ )
$\omega$	Specific dissipation rate
$\varepsilon$	Dissipation rate

### INTRODUCTION

As highlighted in Part I (Ariff et al., 2009), the successful generation of a mesh for a problem domain is an important and integral part of a Computational Fluid Dynamics (CFD) study and this takes a significant amount of project time and effort as identified by Jinyuan et al. (2006).

A general method for determining the most appropriate mesh configuration is a *grid independence test*, where different meshes are tested until the solution is independent of further mesh refinements, by matching the numerical results to bench mark tests and/or experimental data. This in itself is a time-consuming process.

Turbulence flows are significantly affected by the presence of walls due to the no-slip condition resulting in large gradients in the solution variables in this viscosity-affected region. Gerasimov (2006) emphasized that accurate presentation of the near-wall region is paramount to successful simulations of wall bounded turbulent flows.

Salim and Cheah (2009) succeeded in drawing up recommendations for best mesh practices in two-dimensional (2D) wall bounded turbulent flows, based on the wall  $y^+$  in cases where reliable experimental data may not be available for validation. The study was further explored for a three-dimensional (3D) problem by Ariff et al. (2009) as presented in Part I of the same title. The study covered a comparatively low Reynolds number of 1,870 based on cube height and bulk velocity and concluded that the SA turbulence model with a mesh resolving the viscous sublayer was acceptably accurate. Only two wall  $y^+$  ranges were studied and the log-law region was not accounted for, as it would have compromised the overall solution due to the coarser grid. The recommendations include the behaviour and suggested usage of the inbuilt Reynolds averaged Navier-Stokes (RANS) models and near-wall treatments in Fluent.

Part II, as presented here, makes up for the shortcoming with a higher Reynolds number, where the log-law region is also resolved, hence allowing investigation of the behaviour of turbulence models and near wall-treatment for all three wall  $y^+$  (Fluent, 2005):

- $y^+ < 5$  : in the viscous sublayer region  
(velocity profile is assumed to be laminar and viscous stress dominates the wall shear)
- $5 < y^+ < 30$  : buffer region  
(both viscous and turbulent shear dominates)

- (c)  $30 < y^+ < 300$  : Fully turbulent portion or log-law region (corresponds to the region where turbulent shear predominates)

The wall  $y^+$  [equation (1)] is a non-dimensional number similar to local Reynolds number, determining whether the influences in wall-adjacent cells are laminar or turbulent, hence indicating the part of the turbulent boundary layer that it resolves.

$$y^+ = \frac{u_{\tau air} y}{\nu_{air}} \quad (1)$$

A 3D cube immersed in a turbulent channel flow is widely studied due to its simple geometry but the flow contains complex flow structures that characterize numerous configurations relevant to many engineering applications such as wind loading on structures and cooling of electronic components. Martinuzzi and Tropea (1993) and Hussein and Martinuzzi (1996) performed extensive experimental studies on wall mounted cubic obstacles placed in a fully developed turbulent channel flow at high Reynolds number of 40,000. Similarly, a number of numerical analyses exist on the same problem, such as Lakehal and Rodi (1997) employing two-layer turbulence models, Shah and Ferziger (1997) using large eddy simulation (LES), and unsteady flow simulation using Reynolds Averaged Navier-Stokes (RANS) by Iaccarino et al. (2003), among others.

### MODEL DESCRIPTION

The computational domain shown in Figure 1 is identical to that used by Lakehal and Rodi (1997) in their numerical analysis that replicates the experimental setup of Martinuzzi et al. (1993). A fully developed turbulent flow was set at the inlet and  $Re_H = 40,000$ . No-slip conditions were applied on the channel floor, top wall and all cubes faces, whereas the side walls were defined as symmetry to reduce computational cost, since they are sufficiently far from the cube to influence the flow characteristics.

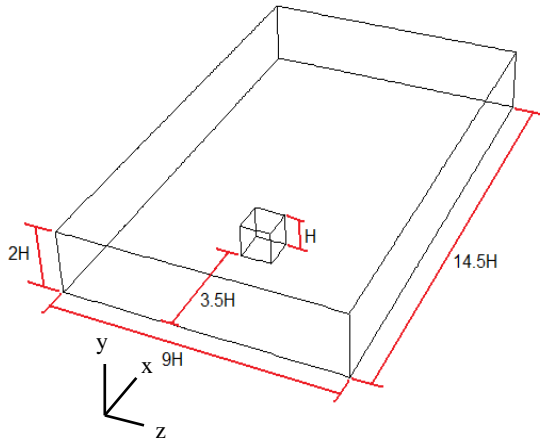


**Figure 1:** Computational geometry of present study.

Incompressible, 3D steady flow RANS equations were implemented to solve the problem and their descriptions are available in the reference texts (Pope, 2000 and Wilcox, 2006). The turbulence closure problems were accounted for using standard  $k-\epsilon$ , standard  $k-\omega$ , RSM, SA and RNG  $k-\epsilon$ . The governing equations for all these models are available in the user guide manual (Fluent, 2005). The pre-processor GAMBIT is used to create the

geometry defining the problem and discretize the domain, while Fluent 6.3 is employed to discretize and solve the governing equations. Figures 2, 3 and 4 show the computational grids with different mesh configurations used for the present study. The height of the wall-adjacent cells for Mesh 1, Mesh 2 and Mesh 3 are  $0.004H$ ,  $0.025H$  and  $0.038H$  resulting in 479,200 cells, 324,960 cells and 181,835 cells, respectively. The successive ratios employed for all the meshes are 1.10, 1.05 and 1.10 in the x-, y- and z-directions, respectively. This allows an analysis of how different turbulence models and accompanying near-wall treatments behave for different regions of resolution as defined by the wall  $y^+$ .

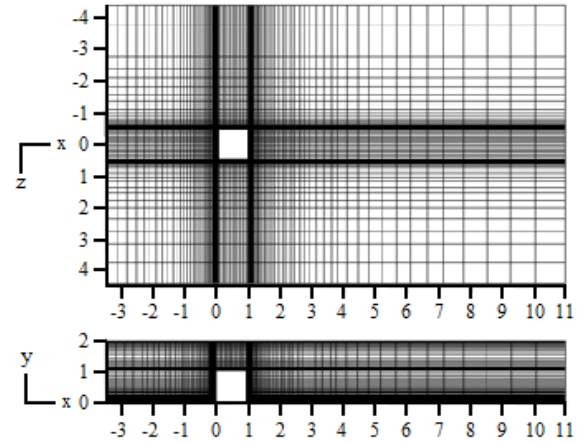


**Figure 2:** Computational grid (Mesh 1) of present study.

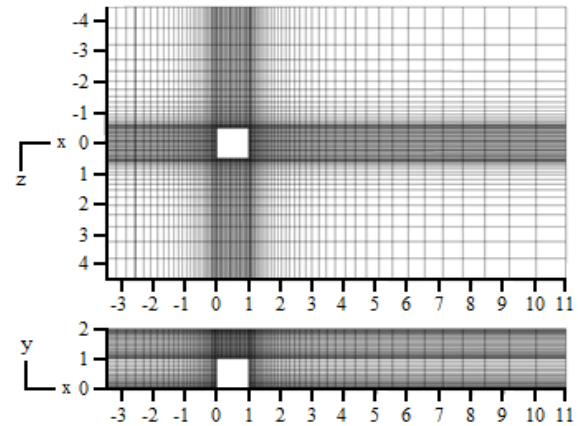


**Figure 3:** Computational grid (Mesh 2) of present study.

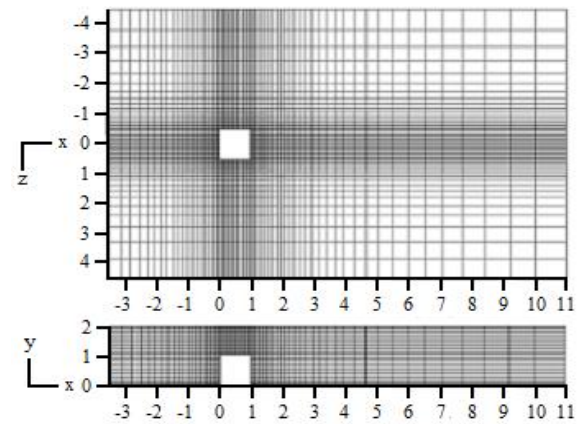


**Figure 4:** Computational grid (Mesh 3) of present study.

## RESULTS

The  $y^+$  values for the three considered meshes are  $\approx 5$ , 22, and 33 corresponding to resolution in the viscous sublayer, buffer region and log-law region, respectively. These are shown graphically in Figure 5.

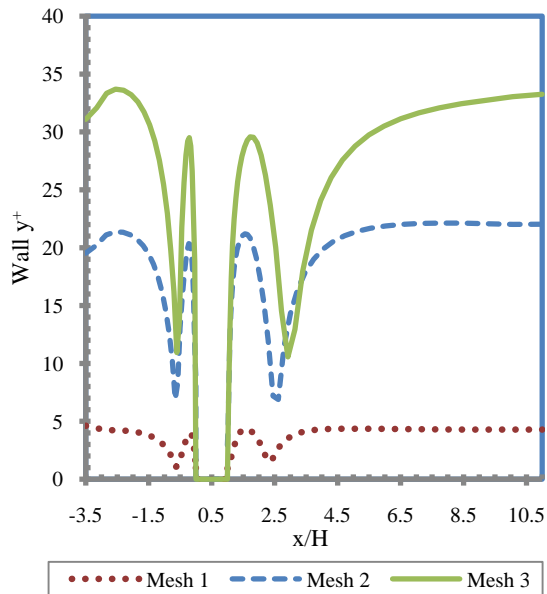


**Figure 5:** Wall  $y^+$  of the considered meshes.

The proceeding results of mean streamwise velocity are presented for different dimensionalized  $x$  distances with ' $x=0$ ' set at the front face of the cube.

Figures 6 and 7 show the comparison of mean streamwise velocity profiles in the symmetry line  $x/H=0.5$  simulated by standard  $k-\varepsilon$  and RSM, respectively. Standard  $k-\varepsilon$  predicted the velocity profiles similarly for all three different meshes. By comparison, the prediction of velocity profiles by RSM was better, noting that the reverse flow is captured near the roof of the cube.

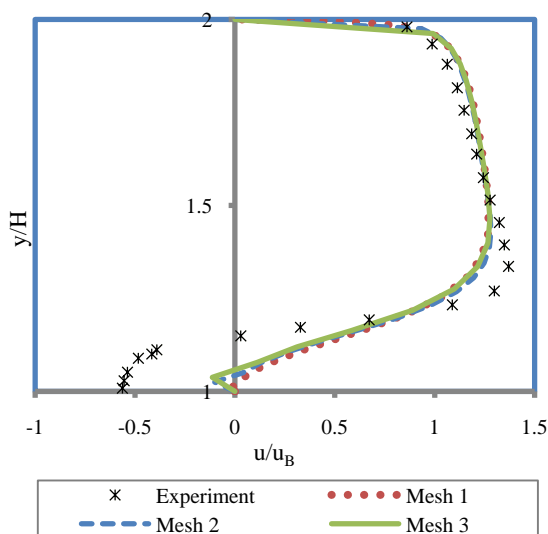


**Figure 6:** Comparison of mean streamwise velocity profiles in the symmetry line  $x/H=0.5$  using Standard  $k-\varepsilon$ , at  $Re = 40,000$ .

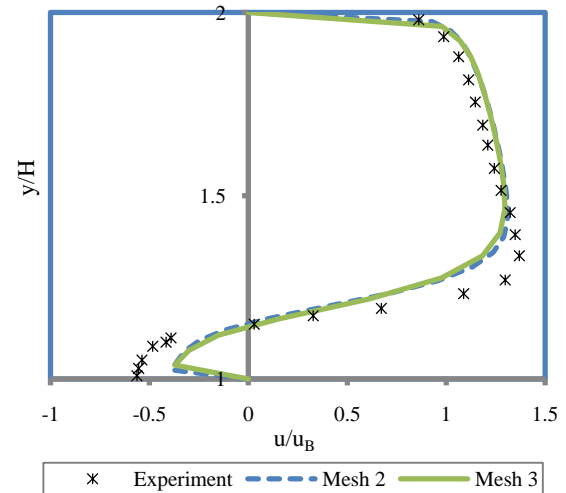


**Figure 7:** Comparison of mean streamwise velocity profiles in the symmetry line  $x/H=0.5$  using RSM, at  $Re_H=40,000$ .

No data for Mesh 1 can be included in Figure 7 as RSM was unable to converge for Mesh 1 with fine grid near the wall ( $y^+ \approx 5$ ). It requires wall functions to bridge the solution variables to the wall, and wall functions do not generally work well in the viscous sublayer as they are formulated using law of the wall which is accurate in the log-law regions only. For Mesh 2 and 3 with wall  $y^+$  values 22 and 33, respectively, RSM predicted the velocity profiles much more accurately. Mesh 2, which resolved a wall  $y^+$  in the buffer region was discarded, following the recommendations in Fluent (2005) that is supported by Salim and Cheah (2009) and Ariff et al. (2009), because neither wall functions nor near-wall modelling accounts for them correctly.

It can be seen that the choice of turbulence model is of minimal significance in the velocity profile calculation for undisturbed flows, as illustrated in Figure 8(a). In Figure 8(b), RNG  $k-\varepsilon$  and RSM agree better with the experimental results in predicting the reverse flow on the top of the cube at  $x/H=0.5$ . RSM is chosen because it accounts for all the Reynolds stresses, unlike the other RANS models that assume them to be isotropic.

Figures 8(d)-8(f) show the mean streamwise velocity profiles downwind of the cube starting with recirculation and leading to reattachment as the flow recovers from separation at the front face and on top of the cube due to an adverse pressure gradient introduced by the cube in the flow path. All RANS turbulence models, particularly RSM and RNK  $k-\varepsilon$ , underpredicted the flow recovery. The simulated flow predicts a larger recirculation region and recovers later than what is observed in the experiment of Martinuzzi et al. (1993). Standard  $k-\varepsilon$  performed comparatively better together with standard  $k-\omega$  model. A similar underprediction of flow recovery was obtained by Lakehal and Rodi (1997) using various versions of the  $k-\varepsilon$  model with an improvement observed by Shah and Ferziger (1997) employing the more computationally expensive LES. DNS results for this flow have not been identified in the literature; possibly due to the computational cost that increases as a factor of the Reynolds number, unlike for the relatively low speed flow of  $Re_H=1,870$  as presented in paper I (Ariff et al., 2009).

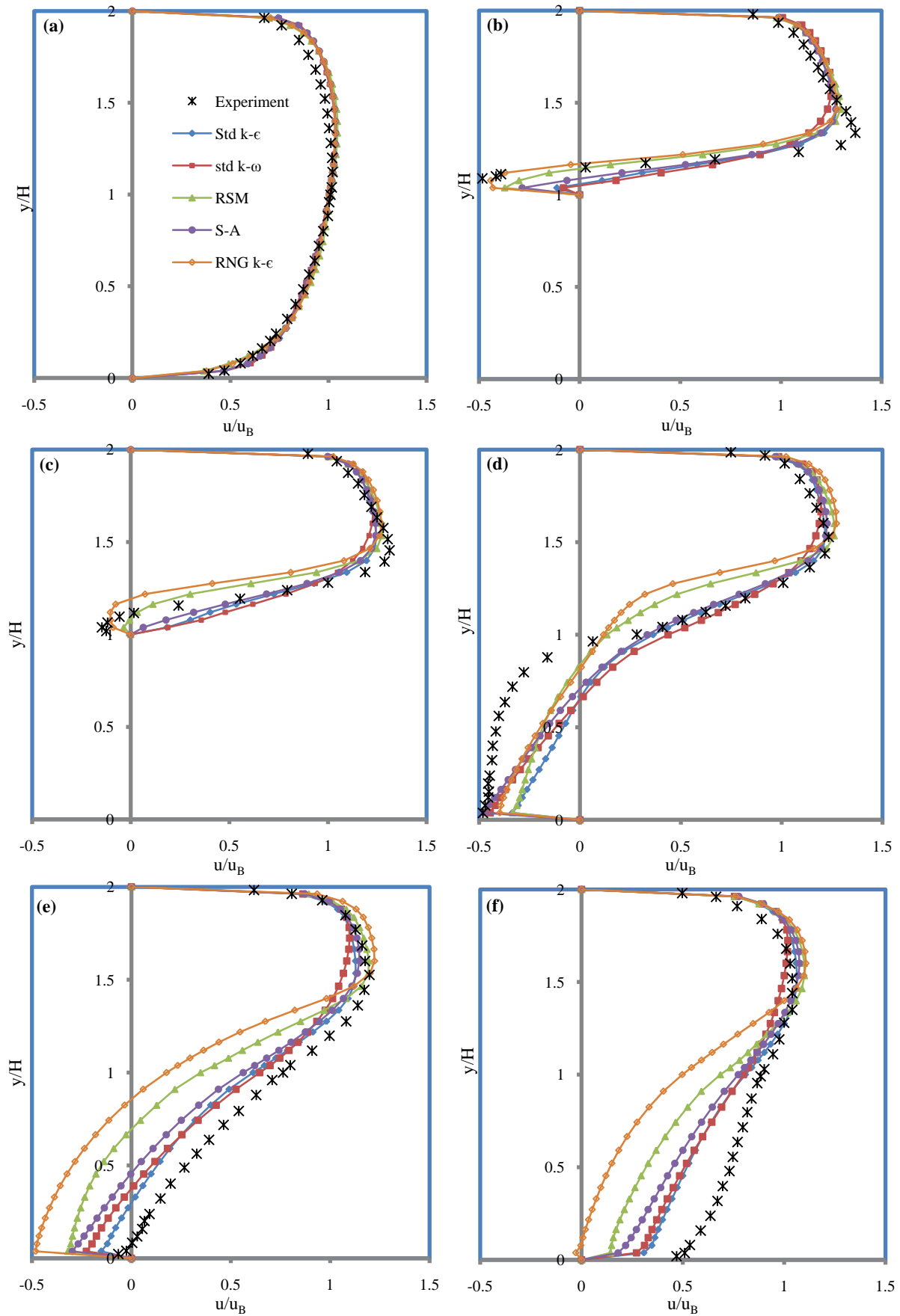
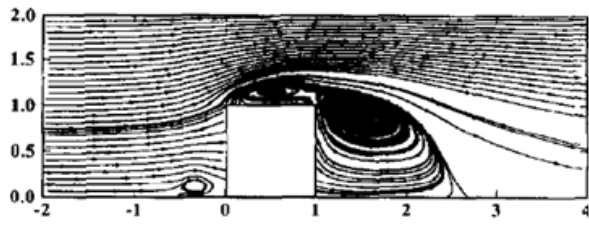
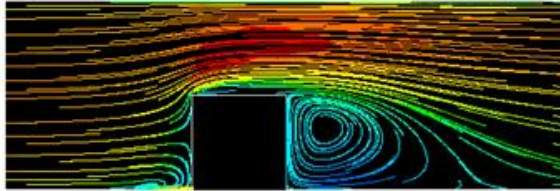
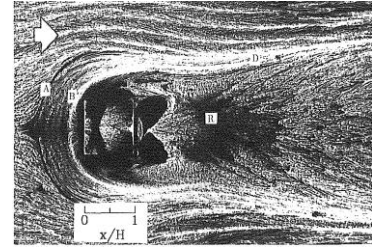


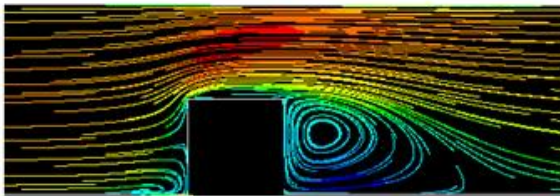
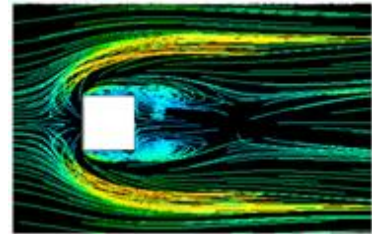
**Figure 8:** Comparison of the mean streamwise velocity profiles of Mesh 3 in the symmetry line (a)  $x/H=-1.0$ , (b)  $x/H=0.5$  (c)  $x/H=1.0$ , (d)  $x/H=1.5$ , (e)  $x/H=2.5$  and (f)  $x/H=4.0$ , for  $Re_H = 40,000$ . Legends are the same in all plots.



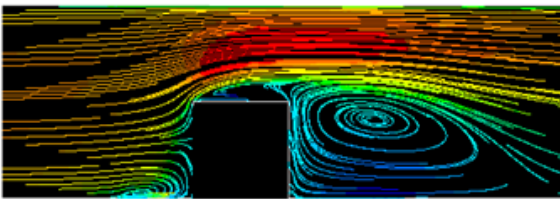
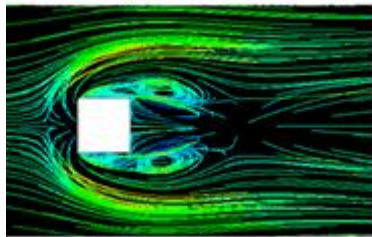
Experiment  
(Martinuzzi et al.,  
1993)



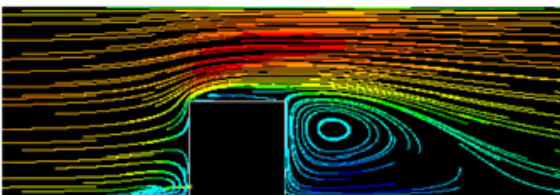
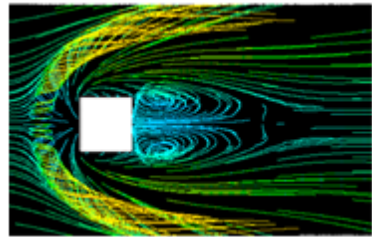
Standard  $k-\epsilon$



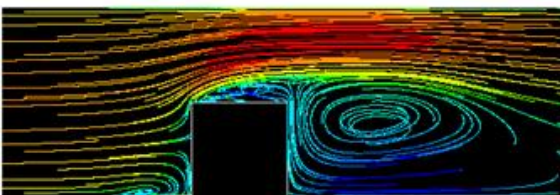
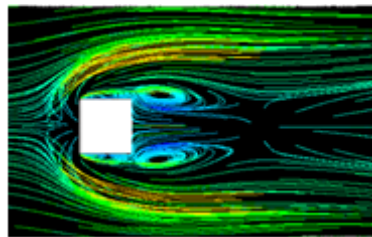
Standard  $k-\omega$



Reynolds Stress  
Model (RSM)



Spalart Allmaras



RNG  $k-\epsilon$

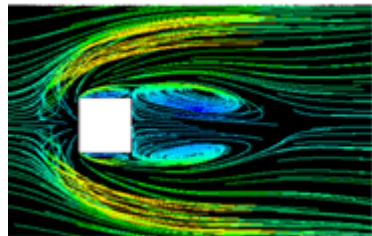


**Figure 9:** Comparison of streamlines in symmetry plane (left)  $z/H=0$  and (right) first cell from bottoms' wall.  $Re_H=40,000$ .

The vortex structures of the flow are investigated by comparing streamlines, generated using different RANS turbulence models in Fluent, with that of the experimental oil-film visualization as illustrated in Figure 9. The separation and recovery regions of the flow can be

compared qualitatively and the most accurate turbulence models can be identified.

For the front and upper separation regions, RSM and RNG  $k-\epsilon$  give better agreement by reproducing a larger vortex

on top of the cube and a front separation length,  $X_F$  closer to the experimental observation. This is supported by the discussion of the velocity profiles as mentioned earlier [See Figure 8(b)].

The flow recirculation behind the cube is overpredicted resulting in a larger reattachment length which consequently underpredicts flow recovery. Standard  $k-\epsilon$  performs better than the other models in capturing this region, with a reattachment length,  $X_R$  nearest to the experimental results, as can be seen in Figure 9 and summarized in Table 1.

Turbulence Models	$X_F(H)$	$X_R(H)$
Experiment (Martinuzzi et al., 1993)	1.040	1.612
Std $k-\epsilon$ (SWF)	0.69	1.98
Std $k-\omega$	0.68	2.05
RSM	0.70	2.40
SA	0.68	2.12
RNG $k-\epsilon$	0.72	2.54

**Table 1:** Summary of front separation ( $X_F$ ) and reattachment lengths ( $X_R$ ) for a wall mounted cube by different turbulence models.

## CONCLUSION

Although the steady RANS turbulence models are not capable of reciprocating exactly the solutions of complex flow structures they do provide CFD results of acceptable agreement to experimental observations, thus enabling their implementation in the design stage and as an aid in product development. It is noted that the accuracy of the computed results are dependent on a number of solver variables such as mesh configuration, numerical schemes, convergence criteria, under-relaxation factors and turbulence models employed. This study has drawn recommendations for the best mesh configuration, coupled with the appropriate turbulence models and near-wall treatment, based on the computed wall  $y^+$  for wall-bounded turbulent flows using the commercial package Fluent.

In Part I of the same title, only two  $y^+$  were investigated due to the relatively low Reynolds number. A mesh configuration with the wall  $y^+$  resolving the viscous sublayer together with Spalart-Allmaras turbulence model was determined to be most appropriate for such low Reynolds number flows.

In this study, based on a much higher Reynolds number of 40,000, Mesh 3 with a wall  $y^+ \approx 33$  resolving the log-law region is sufficiently accurate incurring a lower computational cost as opposed to working into the viscous sublayer. It is also advisable to avoid resolving the buffer

region, as neither wall-functions nor near-wall modelling account for it accurately.

It is observed that for fluid problems with complex turbulent flow structures, e.g. separations and recirculation bubbles, most steady-flow RANS turbulence models are able to predict the flow broadly to an agreeable extent. However, different flow regions have different ‘best’ models for their flow prediction. RSM predicts best the separation region upwind and above the cube, whereas standard  $k-\epsilon$  computes flow results with the least errors in the reattachment/recovery regions.

## REFERENCES

- ARIFF, M., SALIM, S.M., and CHEAH, S.C., (2009), “Wall  $Y^+$  Approach for Dealing with Turbulent Flow over a Surface Mounted Cube: Part I – Low Reynolds number”, Proc. Int. Conf. on CFD in the Minerals and Process Industries, CSIRO, Melbourne, Australia, December.
- FLUENT (2005), *Documentation: User guide*, ANSYS Inc.
- GERASIMOV, A., (2006), “Modelling Turbulent Flows with Fluent”, Europe, ANSYS Inc.
- HUSSEIN, H.J., and MARTINUZZI, R.J., (1996), “Energy Balance for Turbulent Flow around a Surface Mounted Cube Placed in a Channel”, Phys. Fluids 8 (3), 764-780.
- IACCARINO, G., OOI, A., and BEHNIA, M., (2003), “Reynolds averaged simulation of unsteady separated flow”, Int. J. Heat and Fluid Flow 24, 147-156.
- JINYUAN, T., GUAN, H.Y., and CHAOQUN, L., (2006), *Computational Fluid Dynamics: A practical Approach*, USA: Butterworth-Heinemann.
- LAKEHAL, D., and RODI, W., (1997), “Calculation of the flow past a surface of a mounted cube with 2-layer turbulence model”, J. Wind Eng. and Ind. Aerodynamics. 67-68, 66-78.
- MARTINUZZI, R., and TROPEA, C., (1993), “The Flow around Surface Mounted Prismatic Obstacles Placed in a Fully Developed Channel Flow”, Trans ASME J. Fluid Eng 115 (1), 85-91.
- POPE, S.B., (2000), *Turbulent Flows*, Second Edition, Cambridge University Press.
- SALIM, S.M., and CHEAH, S.C., (2009), “Wall  $Y^+$  Strategy for Dealing with Wall-bounded Turbulent Flows”. Proc. Int. MultiConference of Eng. and Comp. Scientists, IMECS 2009, Vol II, Hong Kong, March.
- SHAH, K.B., and FERZIGER, J.H., (1997), “A fluid mechanics view of wind engineering: Large eddy simulation of flow past a cubic obstacle”, J. Wind Eng. and Ind. Aerodynamics 67-68, 211-224.
- WILCOX, D.C., (2006), *Turbulence Modelling for CFD*, Third Edition, DCW Industries.